




# An open-source framework for the FE modeling and optimal design of fiber-steered variable-stiffness composite cylinders using water strider algorithm

A. Kaveh<sup>a</sup>, N. Geran Malek<sup>a</sup>, A. Dadras Eslamlou<sup>a</sup>, and M. Azimi<sup>b</sup> 

<sup>a</sup>Centre of Excellence for Fundamental Studies in Structural Engineering, Iran University of Science and Technology, Tehran, Iran; <sup>b</sup>Department of Civil Engineering, University of British Columbia, Vancouver, BC, Canada

## ABSTRACT

As the automated fiber placement (AFP) manufacturing technology is developed, curvilinear fiber path composite structures received extensive attention. Therefore, developing a design framework capable of optimizing such structures is a significant challenge for researchers and engineers in this domain. In this article, an open-source ABAQUS/MATLAB-based framework is developed for the bending-induced buckling design of variable-stiffness (VS) composite cylinders made using the AFP method. The framework is based on an interface between ABAQUS FE packages with MATLAB environment using Python scripting language. In this framework, the optimized fiber angle distribution of steered plies and associated bending-induced buckling load of its FE model is obtained by applying a meta-heuristic optimization algorithm. The developed Python script submits dimensions, angle distributions, as well as loading and boundary conditions to ABAQUS/CAE. This framework can be customized to meet industrial demands. To show such flexibility, different types of metaheuristic optimization algorithms and aspect ratios are applied, and the associated problems are optimized separately. In addition to the simplicity and versatility of the proposed framework, the results indicate the higher performance of a novel metaheuristic, the so-called Water Strider Algorithm (WSA). Moreover, this framework can be used for finite element modeling and analysis in the metamodeling step for composite cylinders with higher aspect ratios.

## ARTICLE HISTORY

Received 23 June 2020  
Accepted 7 October 2020



## KEYWORDS


Design optimization; fiber placement; variable-stiffness composite cylinder; water strider algorithm; computational framework

## 1. Introduction

Composite structures are widely used as the load-carrying components of automotive structures because these components possess excellent mechanical properties as well as weight efficiency. Their functionality is related to a diverse range of features and parameters involved in designing these structures. Due to numerous advantages over isotropic materials, such as high stiffness, superior features in strength, lightweight, and directional properties, laminated composites are used in several industrial structures (Paris 2009; Shahgholian-Ghahfarokhi et al. 2020).

There are two main strategies for designing laminated structures. First, composite structures are designed as a permutation of several straight-fiber plies called constant-stiffness (CS) composite design. In this kind of problem, there is just one variable in every lamina of the structure, i.e.

**CONTACT** A. Kaveh  [alikaveh@iust.ac.ir](mailto:alikaveh@iust.ac.ir)  Centre of Excellence for Fundamental Studies in Structural Engineering, Iran University of Science and Technology, Tehran 16844, Iran.  
Communicated by Corina Sandu.

 Supplemental data for this article can be accessed at [publisher's website](#).

the constant angle of the fiber. Second, composite structures might be designed for each of the plies as a matrix embracing fibers positioned in the curvilinear paths known as variable-stiffness (VS) design. Each ply could be designed separately in this type of problem since each fiber path could be estimated by multiple numbers of variables (Ghiasi, Pasini, and Lessard 2009; Ghiasi et al. 2010). Along with the above-mentioned variation of fiber angles in CSs structures or fiber paths in VSs, composite laminates may be designed based on other parameters, such as the number of plies and dimensions (Kaveh, Dadras, and Geran Malek 2019a, 2019b). These parameters bring about potential capability in such and other similar composite structures to be tailored and meet the practitioners' and scientists' specific needs.

Due to the advent of automated fiber placement technology (AFP), the uses of VS composites are increased. Accordingly, improving the load-carrying capacity of variable-stiffness structures by optimizing the fiber path has been in the center of attention. In this regard, various continuous path functions have been introduced, such as the linear function that has already been used widely. As the most practical and straightforward fiber path variation, linear variation was proposed in the early stages by Gürdal, Tatting, and Wu (2008). Afterward, other fiber path functions, including trigonometric functions (Blom et al. 2009), cubical and quadratic functions (Muc and Ulatowska 2010), Lagrangian polynomials (Wu et al. 2012), and cubic Bezier curves (Parnas, Oral, and Ceyhan 2003) were also used in the design of VS structures.

AFP is a hybrid manufacturing method with both advantages of automated tape laying and filament winding technologies (Oromiehie et al. 2019). Both plate and cylindrical structures could be fiber-placed using AFP technology. For plate structures, pioneering investigations were conducted by Hyer and Lee (1991) and Gurdal and Olmedo (1993). After that, various experimental, analytical, and numerical methods were adopted for VS panels, most of which are reviewed by Ribeiro et al. (2014). Setoodeh, Abdalla, and Gürdal (2006) demonstrated a substantial increase in the buckling load of variable-stiffness composite plates compared with constant-stiffness design, using lamination parameters methodologies.

White, Weaver, and Wu (2015) studied the buckling and post-buckling behavior of VS cylindrical structures under axial compression. Li (2017) implemented the variable-stiffness properties of the composite cylinders using a user-written subroutine capable of assigning location-based features to every element. In each layer of VS composite structures, the fiber path is a continuous curve, which can be designed in response to the local load-bearing stiffness demand. A multi-step radial basis function (RBF) metamodel-based design approach for maximizing the buckling load of VS cylinders subjected to pure bending was proposed by Rouhi et al. (2017). In their works, at the neighborhood of the optimum points resulted from the previous optimization steps, the side constraints of the design variables are narrowed down. Additionally, sampling, metamodeling, and optimization steps are repeated until convergence is reached. A similar design approach was used to tailor the buckling behavior of laminated composite elliptical cylinders subjected to compressive axial (Rouhi et al. 2016) and bending (Ghayoor et al. 2017) loads. Rouhi et al. (2015) developed a multi-objective optimization to investigate the effect of the variation in bending load direction on the buckling performance of composite cylinders.

Developing straightforward approaches for the efficient design of structures would be a worthwhile effort. In this regard, for instance, Zuo (2013) developed a GA-based optimization software and object-oriented graphics interface design for the cross-sectional shape of thin-walled beams in the automobile body. Tazowski, Blachowski, and Lógó (2019) proposed a new approach to finite element classes implementation benefiting smaller hierarchy. As another example, an object-oriented MATLAB toolbox, based on the transfer stiffness matrix method, was developed by Qin et al. (2017) to promote automotive body-in-white structure design. This study continues the current authors' previous research on a framework developed for the optimization of laminated composite plates (Kaveh et al. 2020). Taking into account that there is not available any convenient, user-friendly approach for numerical modeling and optimization of VS cylindrical

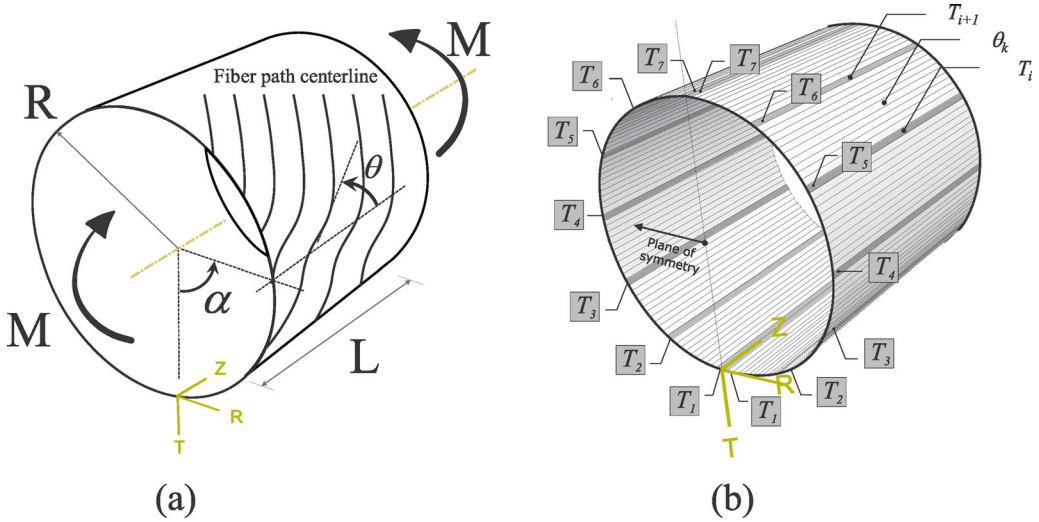


**Figure 1.** Bending-induced buckling of variable-stiffness composite cylinder: (a) Configuration of the composite cylinder with the coordinate system and dimensions, subjected to pure bending loads, (b) piece-wise constant orientation angle narrow section.

composites, the main goal of this study is to develop such a framework. Additionally, this procedure is equipped with a novel metaheuristic for optimizing the orientation distribution of the steered plies. This optimization algorithm encompasses ABAQUS solver, capable of solving non-linear mechanical problems (Geng, Zhao, and Zhou 2020; Hosseini et al. 2020; Qablan et al. 2020), the result of which is considered as the outcome of the objective function for optimization. After verifying the framework based on the available data from the literature, it is used for the buckling design of cylinders with various aspect ratios. Interfacing this algorithm with ABAQUS/CAE is conducted through a Python-script.

This article is organized into five sections. Numerical simulation of the variable-stiffness cylinder FE model is provided in Section 2. The description of the FEM design framework is presented in Section 3. This section represents the MATLAB/Python interface by summarizing the Python code fundamental blocks, followed by a review of two well-known and one novel optimization algorithms. Section 4 aims to show the suitability of the proposed framework by employing it in the problem of cylindrical variable-stiffness composites having various study cases. Eventually, concluding remarks are provided in Section 5.

## 2. Numerical analysis using the finite element method

In this study, the numerical simulations are carried out using ABAQUS software (Systèmes 2010). Figure 1(a) shows the configuration, loading, and coordinate system of the cylinder model with the length and radius of  $L$  and  $R$ . Here, the diameter to thickness ratio of the cylinders is low, and so the thin-walls hypothesis can be used. It should be noted that the cylinders with moderate and thick walls behave differently from the thin wall cylinders because of the influence of shear stresses and lower stiffness. The linear buckling model is utilized here. However, in thick cylinders, reinforcing layers are prone to delamination failures that cannot be captured with the linear, geometric warping model (Ehsani and Rezaeepazhand 2016; Alidoost and Rezaeepazhand 2017).

To apply the concept of the variability of stiffness to cylindrical composite, it must be partitioned into a certain number of narrow sections (see Fig. 1(b)).  $[0^\circ, \theta^\circ, 90^\circ, -\theta^\circ, -\theta^\circ, 90^\circ, \theta^\circ, 0^\circ]_s$  (symmetric 16-ply laminate) is the laminate layups of each of these narrow sections, where  $\theta$  plies are the plies whose direction needs to be steered. The values of design variables  $T_i$  s and therefore  $\theta_k$

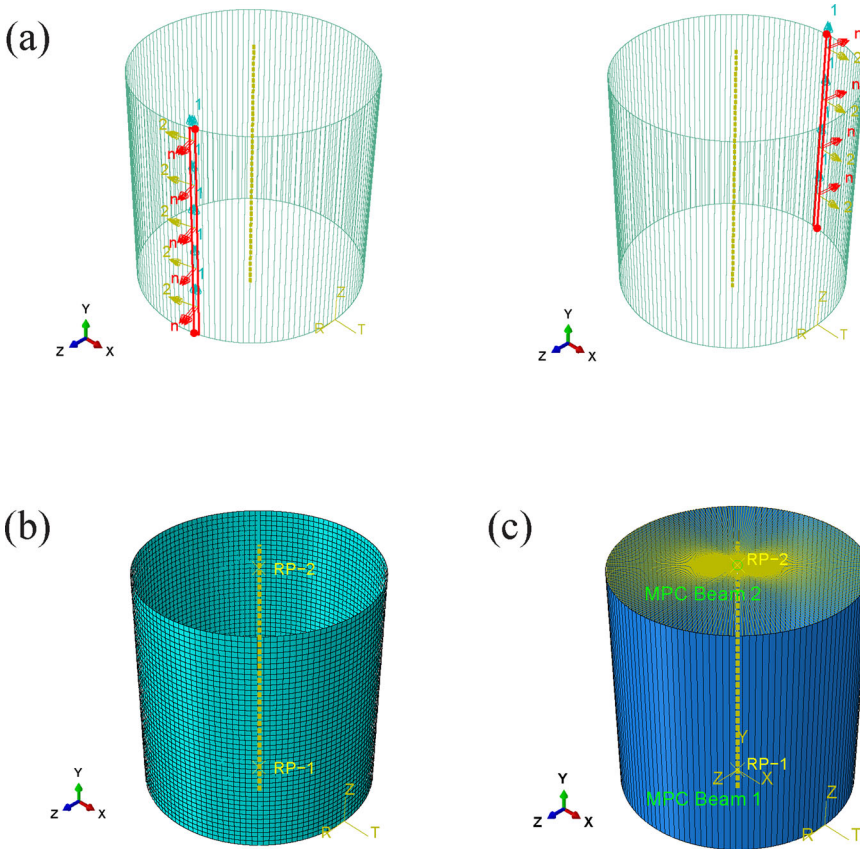


**Figure 2.** Finite element modeling: (a) material orientation, (b) meshing, and (c) MPC constraint.

are assumed to be continuously varied between  $0^\circ$  and  $90^\circ$ . The angle  $\alpha$  determines the spatial location of the narrow sections to which  $\theta$  is assigned. The composite cylinder is symmetrical with respect to the ZT-plane of the coordinate system, as shown in Fig. 1(b). The angles of the fibers are the same in any two narrow sections that are symmetrical about this plane, but with the opposite sign, i.e.  $(\theta = -\theta)$ .  $T_i$   $s$  ( $i = 1, 2, \dots, 7$ ) are the narrow sections whose fiber angles, in one of their plies, constitute seven design variables of the optimization problem, which is discussed further in the following section. The changes in the fiber angles of the rest of the sections are considered as linear.

Moreover, the buckling behavior of the composite cylinder is analyzed. Critical buckling moments of the present optimization problem are calculated via ABAQUS/CAE, by which Lanczos eigensolver is employed to obtain the critical buckling loads and mode shapes.

For each of the narrow sections, the orientation of the material must be defined separately (Fig. 2(a)). The material orientation of each narrow section should be defined in reference to the RTZ datum cylindrical coordinate system. In this figure, the direction of axis 2 remains the same when rotating around the cylinder's circumference. "S8R5" element type, as shown in Fig. 2(b), is used to execute the finite element analyses, in which each element has 8-node of five degrees of freedom. Material characteristics and meshing are assigned according to the modeling procedure studied by Rouhi et al. (2017). Five thousand seven hundred and sixty-two number of quadratic quadrilateral elements of type S8R5 are generated with the approximate global size of 10.6, in which on every top and bottom edges of the 134 sections, only one seed is assigned. To ensure that the circular geometry of the upper and lower edges is preserved during deformation, beam-

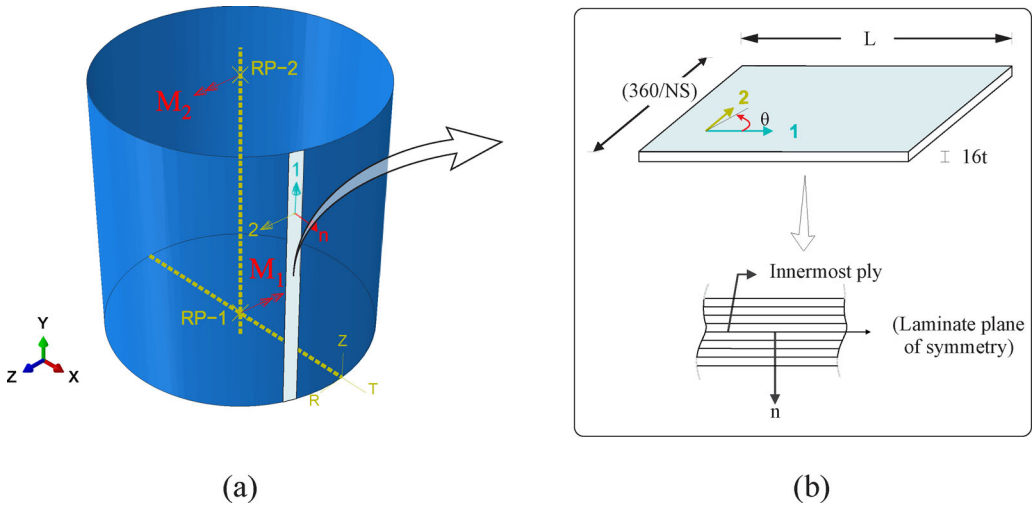


**Figure 3.** Configuration of the variable-stiffness composite cylinders: (a) piece-wise constant model of the variable-stiffness cylinder, (b) laminate fiber path direction and plane of symmetry.

type multipoint constraint (MPC) constraint, as shown in Fig. 2(c), is applied on the top and bottom edges of the cylinder. These constraints tied the circular edge to the central points of their associated endings. The loading in the form of pure bending is applied on both sides of the cylinder.

### 3. Finite element framework

The main goal of the current framework is to interface an optimization algorithm implemented in MATLAB with a Python-script that is connected to the ABAQUS FE solver. The optimization problem is to find the optimum orientation angle distribution  $T_i$  s that result in the maximum possible buckling load capacity. A Python-script does finite element modeling and analysis, and optimization is executed by MATLAB code. Herein, the Water Strider Algorithm (WSA) as a novel population-based and nature-inspired optimization algorithm and two well-known optimization algorithms, namely PSO and GA, are applied to the current problem. From the framework implementation perspective, these optimization strategies could be replaced with other algorithms easily. The entire code of this framework, for a typical verified case, is available in the [supplemental online material](#). Not only the optimization algorithm, but loadings, dimensions, and boundary conditions can be customized to meet the researchers' needs.

#### 3.1. Python-script

The need for a Python-script arises from the automated procedure required for the finite element numerical analysis and iteration-based mechanism of the optimization. For the finite element analysis of the continuity of change in the fiber angles of the steered plies, the circumference of the cylinder must be divided into a limited number of narrow sections. Such simplification is as if the structure is made by connecting a multitude of constant-stiffness laminated composite plates (134, in this study). That results in a number of variables equal to the number of these laminated composite plates. If  $\theta_k$  is the steered ply angle of each of these constant-stiffness plates, the number of variables is reduced by half due to the symmetry of the cylinder relative to the ZT-plane ( $\theta_k = -\theta_k$ ). Doing that is similar to the case where the continuous fiber path is being replaced with a discrete piece-wise constant one having a limited number of design variables.

**Table 1.** Implementation of Python code fundamental blocks.

	# Create model with arbitrary dimension
1.	<pre> NS = 134 # Number of narrow sections L = 457.200012 # Length of the cylinder (L=D=18 in) D = L # Diameter of the cylinder ThicknessOfEachPly = 0.127 # Thickness of each ply MyModel = mdb.Model(name='VS_Cylinder') mdb.models['Model-1'].Material(name='Material_1') mdb.models['Model-1'].materials['Material_1']. Elastic(type=ENGINEERING_CONSTANTS, table=((134000.0, 7710.0, 7710.0, 0.301, 0.301, 0.396, 4310, 4310, 2760), )) mdb.models['VS_Cylinder'].BuckleStep(name='Step-1', previous='Initial', numEigen = 1, eigensolver = LANCZOS, minEigen = 0.0, blocksize = DEFAULT, maxBlocks = DEFAULT) mdb.models['VS_Cylinder'].MultipointConstraint(name='Constraint-1', controlPoint = Region1RefPointBottom, surface = BottomEdge, mpcType = BEAM_MPC, userMode = DOF_MODE_MPC, userType = 0, csys = None) d = p.datums p.DatumCsysByOffset(datumCoordSys = d[Datume_Keys[-1]], Datum_Keys = d.keys() name='MySecond_CSYS', coordSysType = CYLINDRICAL, vector=(D/2, 0.0, 0.0)) for i in range(NS): region = p.sets['NarrowSegment_%d'%(i+1)] orientation = mdb.models['Model-1'].parts['Part- 1'].datums[Datume_Keys[-1]] mdb.models['Model-1'].parts['Part- 1'].MaterialOrientation(region = region, orientationType = SYSTEM, axis = AXIS_2, localCsys = orientation, fieldName='', additionalRotationType = ROTATION_ANGLE, additionalRotationField = '', angle = 0.0) </pre>
2.	# Import material (all properties are given in N, and mm)
3.	# Import step (Buckling with zero as the minimum interested Eigen)
4.	# Create MPC Constraint for the bottom and top circular Edges
5.	# Create cylindrical coordinate system
6.	# Assign material orientation for each narrow sections (NS)

```

7. # Top reference point
a = mdb.models['VS_Cylinder'].rootAssembly
region = a.sets['RefPointSet_Top']
mdb.models['VS_Cylinder'].DisplacementBC(name='BC-RefPointSet_Top',
createStepName='Step-1', region = region, u1 = 0.0, u2 = UNSET, u3 = 0.0,
ur1 = 0.0, ur2 = 0.0, ur3 = UNSET, amplitude = UNSET,
buckleCase = PERTURBATION_AND_BUCKLING, fixed = OFF,
distributionType = UNIFORM, fieldName='', localCsys = None)
# Bottom reference point
a = mdb.models['VS_Cylinder'].rootAssembly
region = a.sets['RefPointSet_Bottom']
mdb.models['VS_Cylinder'].DisplacementBC(name='BC-
RefPointSet_Bottom', createStepName='Step-1', region = region,
u1 = 0.0, u2 = 0.0, u3 = 0.0, ur1 = 0.0, ur2 = 0.0, ur3 = UNSET,
amplitude = UNSET, buckleCase = PERTURBATION_AND_BUCKLING,
fixed = OFF, distributionType = UNIFORM, fieldName='', localCsys = None)
# on bottom RP
mdb.models['VS_Cylinder'].Moment(name='Load-1', createStepName='Step-
1', region = Region1RefPointBottom, cm3 = -1, distributionType = UNIFORM,
field='', localCsys = None)
# on top RP
mdb.models['VS_Cylinder'].Moment(name='Load-2',
createStepName='Step-1', region = Region1RefPointTop, cm3 = 1,
distributionType = UNIFORM, field='', localCsys = None)

# Create boundary condition

# Import load

```



Further simplification could be applied if these  $\theta_k$  variables were reduced to  $T_i$  ( $i = 1, 2, \dots, 7$ ) variables whose narrow sections are placed equally-spaced apart from each other on the circumference of the cylinder. Here, for the rest of the narrow sections between each of the two subsequent  $T_i$ s, fiber angles are also assumed to vary linearly according to Eq. (1):

$$\theta_k = T_i + \frac{\alpha_k - \alpha_i}{\alpha_{i+1} - \alpha_i} (T_{i+1} - T_i); \quad i = 1, \dots, m, \text{ and } k = 1, \dots, n \quad (1)$$

where  $m$  and  $n$  are the number of design variables ( $m = 7$ , in this study) and the number of narrow sections between two subsequent sections having  $T_i$  as their fiber path angle. In the presented codes, the reader can choose either the mentioned linear or spline fit through the seven design points. It should be pointed out that in this study,  $n = 10$ , given that the circumference of the cylinders is divided into 134 number of narrow sections. Overall, the problem of modeling the geometry of the variable-stiffness composite cylinder can be considered similar to the modeling of several constant-stiffness laminated composites that are arranged one after the other, and their fiber angles follow a specific relationship. One such laminated composite, along with its material orientation, is shown schematically in Fig. 3. Material orientation in each laminated composite is implemented by creating the  $1$ - $2$ - $n$  datum coordinate system relative to the previously defined RTZ cylindrical coordinate system. The fiber angle is measured relative to the  $1$ -axis of this local coordinate system (see Fig. 3(b)).

Besides implementing the piece-wise constant concept, Python-script introduces other parameters to the ABAQUS/CAE: dimensions, material properties, boundary condition, material orientation, and applied loads. Bending-induced buckling occurs through applying moment  $M_1$  on a bottom and  $M_2$  on a top reference point as  $M_1 = M_2 = 1$  (N.mm). Moments should be applied such that compression will be exerted on the part of the cylinder located at  $180^\circ$ , given the RTZ coordinate system. Thus, considering the XYZ coordinate system of Fig. 3, the moment applied on the top edge's central point (reference point 1) must be in the  $+z$ -direction, and the moment on the bottom reference point should be in the reversed direction. Pure bending loads were applied at the top and bottom center points of the cylinder, where they tied to their associated circular base edges using beam-type Multipoint constraint (MPC beam). MPC constraint preserves the upper and lower edges of the cylinder circular during any arbitrary deformations. It is to be noted that negative buckling loads were exempt from the analyses ( $\text{minEigen} = 0.0$ ).

Code customizability is further understood by considering lines 1–8 in Table 1. Some fundamental blocks of the Python-script are given in this table, while the entire code can be accessed from the [supplemental online material](#). Lines 1 to 8 show how to model the main parts of the finite element analysis from assigning the dimensions of the cylinder to apply loadings and boundary conditions. After setting the length, diameter, and the number of narrow sections of the cylinder in line 1, material properties of the composite plies are imported in line 2. Then, in lines 3 and 4, the number of desired critical buckling load is asked, and beam-type MPC constraint on the top and bottom edges of the cylinder are defined. RTZ datum coordinate system is specified by offsetting the primary coordinate system located at the center point of the bottom ending (line 5). The orientation of the material, which must be defined separately for each section, is implemented by a `FOR` loop, as given in line 6. For each node, there are three degrees of freedom for displacements and three for rotations. As mentioned in row 7 of Table 1, simply supported-simply supported (SS) boundary condition is applied by allowing the top reference point to move along the centerline of the cylinder ( $U1 = U3 = UR1 = UR2 = 0$ ) and fixing the bottom reference point ( $U1 = U2 = U3 = UR1 = UR2 = 0$ ). Here,  $U_i$  denotes the translational and  $UR_i$  is the rotational degree of freedom in reference to the  $i$  axis. Besides, 1, 2, and 3 represents the direction along the  $x$ -axis,  $y$ -axis, and  $z$ -axis, respectively. In simple terms, for implementing the SS boundary condition, all the rotational and translational degrees of freedoms at the bottom reference point are fixed except for the rotation in the  $z$ -direction. Also, the



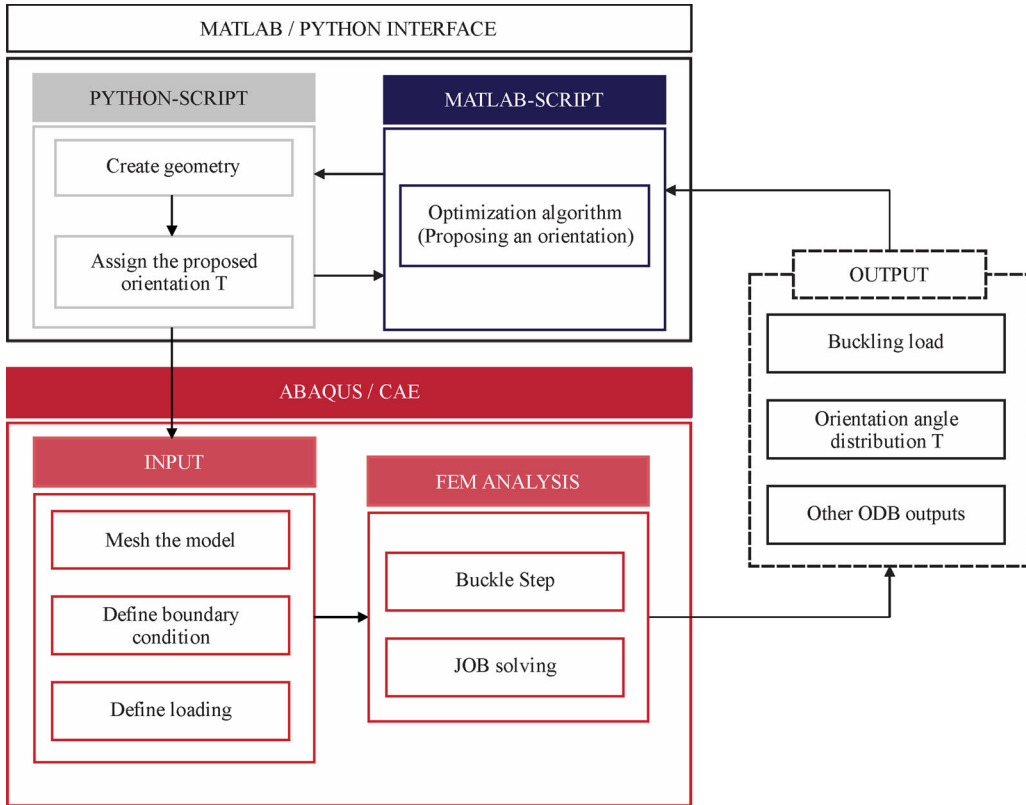


Figure 4. Flowchart of the FE-based framework.

translation of the top reference point in the  $y$ -direction and rotation around the  $z$ -direction is allowed. This boundary condition can also be changed to other types of boundary conditions, such as simply supported-fixed, fixed-simply supported, and fixed-fixed, in case they are the desired boundary conditions (Hu and Chen 2018). Moreover, loadings could be changed into a desirable one such as concentrated force, thermal, displacements, and pressure, by replacing them with line 8.

As shown in the MATLAB/ABAQUS interface flowchart of Fig. 4, the framework acts such that ABAQUS is the solver for every single analysis of the objective function. Once the framework starts running, for every single execution of the objective function, Python-script creates a folder with the same name in which it stores the associated model and its produced outputs (as shown in ABAQUS/CAE block of Fig. 4). When a FE function evaluation, three text files are generated to store the information for the proposed orientation angle distribution  $T$ , critical buckling moment, and overall layup angles. Then, the objective function, i.e. the critical buckling load value, is read by MATLAB, and according to its essence of the optimization algorithm, a new orientation angle distribution  $T$  is proposed. These recursive processes, which are shown in Fig. 4 using cyclic arrows, continues until the termination condition of the optimization algorithm is satisfied.

### 3.2. Optimization strategies

Limitations of gradient-based methods, such as convergence to localized minima or high dependency on the initial solution, have led to the increasing use of metaheuristic algorithms. Due to

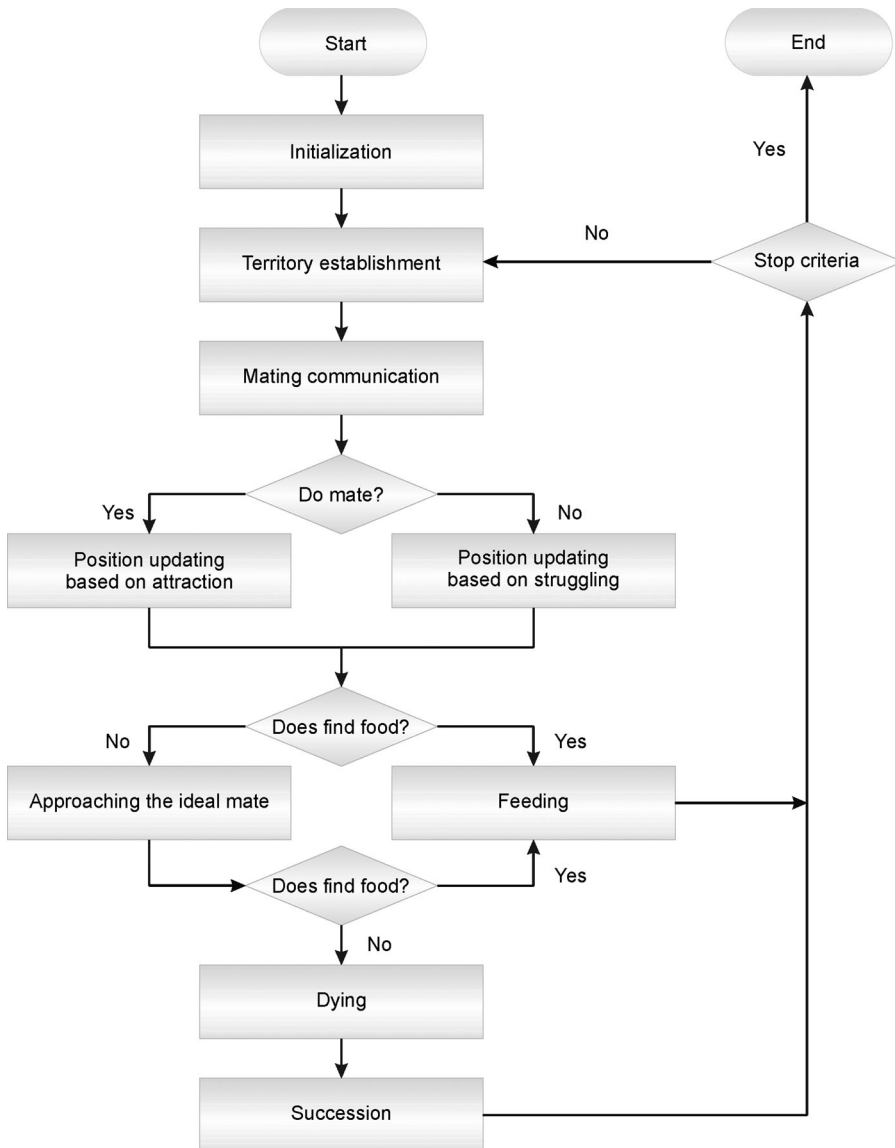


**Figure 5.** Flowchart of the WSA algorithm.

their capability to find and explore the promising regions with reasonable computational effort, metaheuristic algorithms are suitable for global searches over the entire search space. Some of the applications of these algorithms and their implementations can be found in the literature (Kaveh and Dadras Eslamlou 2020a, 2020b).

### 3.2.1. A brief overview of the WSA algorithm

Water strider algorithm (WSA) is a novel population-based swarm intelligent optimization algorithm inspired by water striders' life cycle. WSA mimics intelligent ripple communication, territorial behavior, mating style, succession, and water striders' feeding mechanisms. These strategies were implemented with an attempt to utilize mathematically simple formulations representing the life cycle of water striders by Kaveh and Dadras Eslamlou (2020a, 2020b).

Due to the hydrophobic legs of WSs and surface tension of the water, this family of animals has achieved a natural ability to live on top of the water. For female water striders, defending from food resources, and for male striders, protecting from their mating partners is the reason why the striders establish a territory for themselves. Each territory is usually inhabited by a couple of female striders and one male so-called ‘keystone’ strider. By oscillating their legs on the top surface of the water, the striders produce ripples with different frequencies, durations, and amplitudes, by which they could convey different types of information with one another. Depending on the features that each signal possesses, a different type of information is sent out, such as repelling the invader, positioning the prey, and courtship. Incoming signals are received through a sensory receptor organ on their legs. This organ can also distinguish signals that are being produced by prey insects trapped on the surface of the water. The pre-copulatory calling signal transmitted by a male insect will be responded by a negative or positive message from the female insect. Based on that feedback, the striders will update their positions as given in Eq. (2):

$$\begin{aligned} WS_i^{t+1} &= WS_i^t + R \cdot rand ; \text{ Positive response} \\ WS_i^{t+1} &= WS_i^t + R \cdot (1 + rand); \text{ negative response} \end{aligned} \quad (2)$$

where  $WS_i^t$  is the position of  $i$ th WS in the  $t$ th cycle, and  $rand$  is a random number between 0 and 1. Also,  $R = WS_F^{t-1} - WS_i^{t-1}$ .

The exploitative, exploratory, convergence, local optima avoidance, and other proposed algorithm features were studied by applying it on a large number of multimodal unimodal, shifted, biased, and composite functions. Besides, the WSA is employed successfully in numerous continuous, constrained, discrete, and unconstrained engineering design problems (Kaveh and Dadras Eslamlou 2020a, 2020b). The flowchart of the WSA is illustrated in Fig. 5. A comprehensive description of the WSA is provided in Kaveh and Dadras Eslamlou (2020a, 2020b).

### 3.2.2. A brief overview of genetic algorithm (GA)

The genetic algorithm (GA), which is derived from the theory of Darwin, is first developed by Holland (1992). As the most common optimization method used in the broad range of engineering problems (Khalkhali, Ebrahimi-Nejad, and Malek 2018), GA is inspired by the evolution of biological individuals. Crossover, mutation, survivor selection, and parent selection are the leading operators (Sivanandam and Deepa 2008).

GA comprises two essential steps, including initialization and the main loop of the algorithm. The critical task that GA undertakes is to produce a highly evolved version of the population from a random initial solution with its operators and selection mechanisms. In the initialization phase, random chromosomes for the first generation are produced ( $nPop$ ). This part of the code runs outside the main loop. However, in the main loop, crossover and mutation operations are performed as large as the population designated based on the crossover and mutation probability ( $nc + nm$ ). All of these populations ( $nPop + nc + nm$ ) are then sorted according to the value of their objective functions. The function evaluation of these populations is conducted using the ABAQUS FE Package. Every time the objective function is called, it executes the Python code. This step is carried out through what was described in Section 3.1 on interfacing MATLAB environment with ABAQUS FEA software using Python-script.

After sorting, populations should be truncated; therefore,  $nPop$  number of populations being remained. To randomly select two parents among the  $nPop$  available parents tournament selection is utilized to produce offspring.

In this article, 80% of the populations are selected for the *crossover* operation. Besides, to keep the biological diversity that is an essential feature of the genetic algorithm, in a step called *mutation*, 20% of the populations are being mutated. In contrast to crossover that results in producing two offspring from two random parents, in mutation, a random parent is being mutated,

**Table 2.** Material properties of unidirectional carbon/epoxy composite ply (Barbero 2013).

Property	AS4D/9310
$E_1$	134 GPa
$E_2 = E_3$	7.71 GPa
$G_{12} = G_{13}$	4.31 GPa
$G_{23}$	2.76 GPa
$\nu_{12} = \nu_{13}$	0.301
$\nu_{23}$	0.396
Thickness of each ply (t)	0.127 mm

resulting in one child. The total number of parents is not going to be considered as it needs to sort and truncate them to have  $nPop$  number of populations.

### 3.2.3. A brief overview of PSO algorithm

Developed by Kennedy and Eberhart (1995), PSO is a swarm intelligence optimization technique that is inspired by the social behavior of animal packs, such as fish schools or bird flocks. It starts with random initialization of a swarm (population) of particles (individuals) in a search space of  $n$ -dimension, which is the problem's dimension. Position  $x_i = (x_1, x_2, \dots, x_n)$  and velocity  $v_i = (v_1, v_2, \dots, v_n)$  are the two features by which every particle  $i$  is characterized. Besides these features, each particle holds the memories of its best personal experience  $P_i$  and the best group experience  $P_g$ . In other words,  $P_i$  and  $P_g$  represent the best previous position of each individual as well as all of them, respectively. Here, the best position means the location at which the objective function reached the maximum (optimum) value. The value of the objective function associated with these positions are called  $P_{best}$  and  $g_{best}$ , respectively. These particles are moved from the position  $x_i^t$  with velocity  $v_i^t$  to a new position  $x_i^{t+1}$  whose velocity is  $v_i^{t+1}$ , according to the following relationships:

$$\begin{aligned} v_i^{t+1} &= \omega v_i^t + c_1 r_1 (p_i^t - x_i^t) + c_2 r_2 (p_g^t - x_i^t) \\ x_i^{t+1} &= x_i^t + v_i^{t+1} \end{aligned} \quad (3)$$

where  $r_1$  and  $r_2$  are uniformly distributed random numbers in the interval  $[-1, 1]$ . Also,  $c_1$  and  $c_2$  are acceleration constants changing the velocity of a particle toward the best individual experience and the best group's experience, respectively. In other words, these coefficients determine how much a particle follows cognitive and social components, respectively. Delving further into that, when the value of  $c_2$  decreases, particle  $i$  tends to move more toward  $p_i^t$  than  $p_g^t$ , and vice versa. Besides the direction to which the particles should move, it must be available a factor that controls how much this movement should be. This factor, which controls the amount of exploitation and exploration of the search space, is called inertia weight factor  $\omega$ . The higher amount of this factor results in more new areas to be searched by the particles, and vice versa (Moussavian and Jafari 2017).

## 4. Verification of the framework

The performance of the presented FE approach is verified by comparing the obtained buckling load capacity of the QI and VS cylinders with their counterparts in Rouhi et al. (2014, 2017). The validity of the numerical FE simulation and the proposed optimization framework is shown with the QI and VS cases, respectively. The cylinders have simply supported-simply supported boundary conditions, and constant length  $L$  as well as diameter  $D$ , where  $L = D = 457.2$  mm. A 16-ply symmetric, balanced having stacking sequence of  $[0^\circ, \theta^\circ, 90^\circ, -\theta^\circ, -\theta^\circ, 90^\circ, \theta^\circ, 0^\circ]_s$  is considered as the layup of VS composite cylinder. Plies with an angle of  $\theta$  are regarded as the

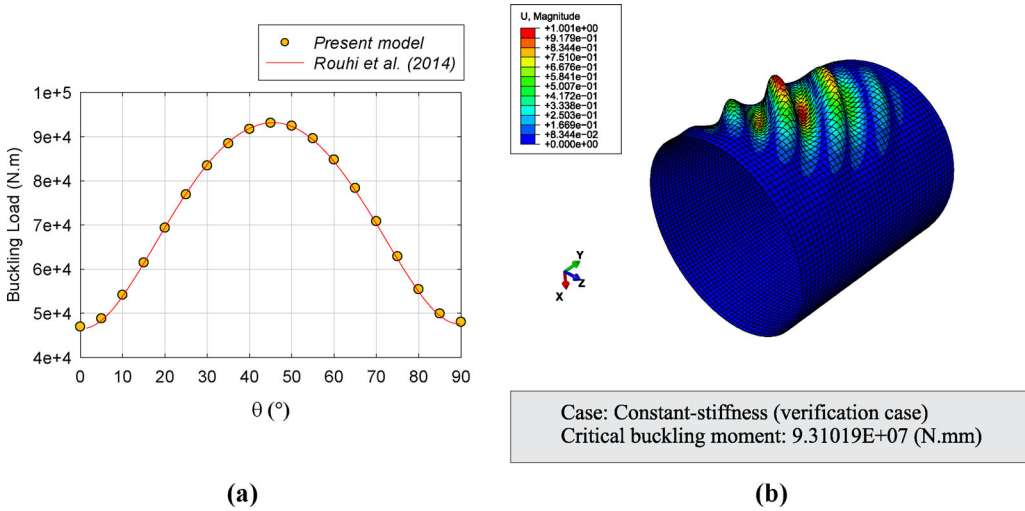


**Figure 6.** Verification of presented FE approach for QI composite cylinder ( $\frac{L}{R} = 2$ ): (a) buckling loads at different values of  $\theta$  (for every  $5^\circ$  angle), (b) mode shape of the verified case for  $\theta = 45^\circ$ .

candidate plies that need to be fiber-steered such that the bending-induced buckling reaches its maximum value. Buckling is induced by the pure bending load of  $M_1 = M_2 = 1\text{N mm}$  applied to the reference points at the top and bottom of the cylinder. Mechanical properties of AS4D/9310 lamina are taken as the material properties (Table 2).

The same layup is considered for the constant-stiffness composite cylinder. Constant-stiffness cylinder comprises of several narrow sections whose  $\theta$  values are the same. For the case of a constant-stiffness composite, the buckling moment is verified for several constant values of  $\theta$  between 0 and 90. As can be seen from Fig. 6(a),  $\theta$  is changed in every  $5^\circ$  interval from  $0^\circ$  to  $90^\circ$ . As shown in this figure, the maximum bending moment that the cylinder could withstand is achieved when all narrow sections have a fixed steered ply angle of  $45^\circ$ . Moreover, as the  $\theta$  angle of these sections deviates from  $45^\circ$ , the cylinder buckles at lower loads. Therefore,  $[0^\circ, 45^\circ, 90^\circ, -45^\circ, -45^\circ, 90^\circ, 45^\circ, 0^\circ]_s$  is the optimum stacking sequence of all the narrow sections comprising the QI cylinder. The mode shape associated with this layup is presented in Fig. 6(b).

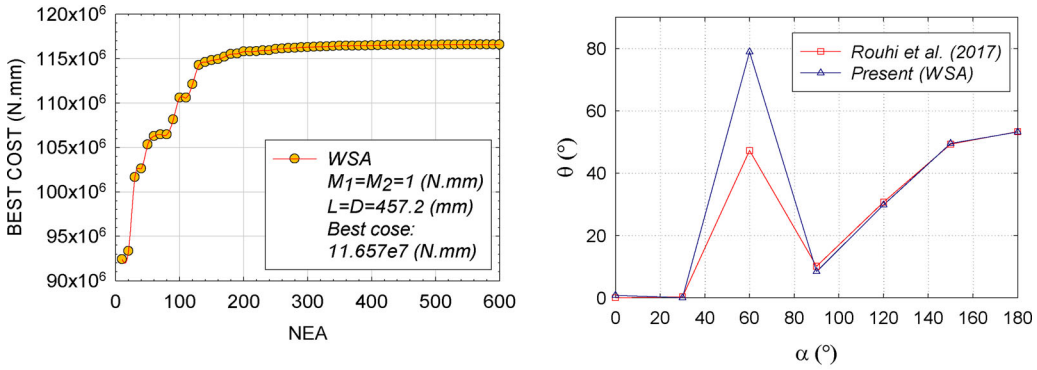
After the verification of the FE analysis for the QI case, to verify the optimization performance of the framework, the VS design is carried out as well. Boundary conditions, dimensions, and loading are the same as the case of the QI cylinder. However, as  $\alpha$  varies between  $0^\circ$  and  $180^\circ$ , around the circumference of the cylinder,  $\theta$  is not constant, and it undergoes seven discontinuous changes. These changes in the value of  $\theta$  occur at seven, specific narrow sections whose  $\theta$  values are identified by  $T_1$  to  $T_7$ . Once again, to show the validity of the FE modeling, this time for the VS case, for the same values of the  $T_i$  reported in Rouhi et al. (2017), buckling load is obtained, which shows a good agreement, as given in Table 3.

As shown in Fig. 7, with a population size of 10 and 600 number of eigenvalue analyses (NEA), buckling load is optimized. The optimum verified orientation angle distribution of the steered plies and the buckling mode shape of the converged composite cylinder are shown in Figs. 7(b) and 7(c), respectively. The distinct difference between the values of  $T_3$  appears from the better buckling load that the framework is converged to. It is noteworthy that, for both of the QI and VS cylinders, there is a line in the Python-script through which other desirable stacking sequences could be implemented by modifying it as follows:

```
myOrientationsList[i].extend([0,tetta[i],90,-tetta[i],-tetta[i],90,tetta[i],0])
```

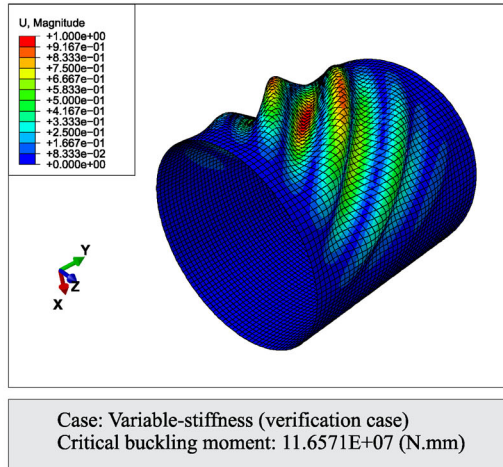
**Table 3.** Buckling load of the QI and VS composite cylinders ( $D = L = 457.2$  mm).

Composite cylinder	Buckling load (N mm)	
	Rouhi et al. (2017) ( $\times 10^7$ )	Present study ( $\times 10^7$ )
QI	9.32	9.31
VS	11.64	11.641



(a)

(b)



(c)

**Figure 7.** Verification of presented FE framework for VS composite cylinder ( $\frac{L}{R} = 2$ ): (a) converged buckling load after 60 number of iterations and population size of 10, (b) optimum orientation angle distribution of the steered plies, (c) mode shape of the optimized model.

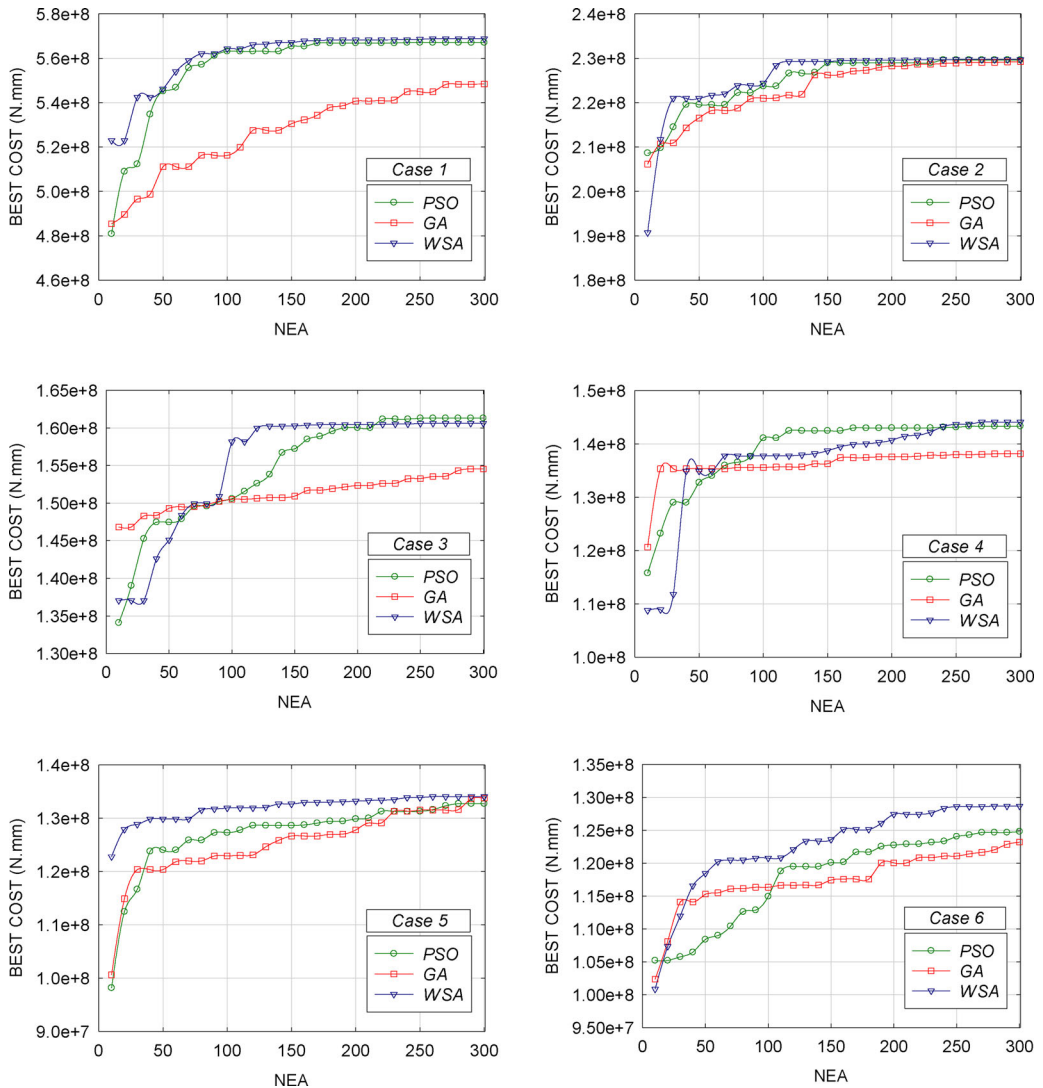
## 5. Numerical results and discussions

For a thin structure, structural performance may be influenced by the length to radius aspect ratio ( $L/R$ ). To examine the effect of aspect ratio, the length of the cylinder is changed while the radius and thickness of the cylinder are kept constant. The current section studies the impact of different aspect ratios of the cylinder on the optimized orientation angle distribution and critical buckling load of the VS composite cylinders. Simply supported-simply supported boundary condition is considered as the boundary conditions of the cylinders. These composite cylinders are subjected to pure bending moments of  $M_1$  and  $M_2$  at both sides, where  $M_1 = M_2 = 1$  N mm. The radius of the cylinder at the top and bottom ends are equal to 457.2 mm. However, the



**Table 4.** Optimized buckling load (N.mm) of variable-stiffness cylinders for different optimization algorithms along with QI cylinders at different aspect ratios ( $R = 457.2$  mm).

Case	$L/R$	$QI (\times 10^7)$	Rouhi et al. (2014) ( $\times 10^7$ )	$PSO (\times 10^7)$	$GA (\times 10^7)$	$WSA (\times 10^7)$
1	0.1	41.160	50.169	56.706	54.842	<b>56.881</b>
2	0.2	16.743	22.254	22.963	22.923	<b>22.971</b>
3	0.3	12.325	15.844	<b>16.129</b>	15.454	16.061
4	0.4	11.235	14.169	14.333	13.816	<b>14.411</b>
5	0.5	10.542	13.308	13.273	13.378	<b>13.407</b>
6	0.6	10.073	12.844	12.480	12.319	<b>12.867</b>
7	0.7	9.807	12.346	12.516	12.259	<b>12.518</b>
8	0.8	9.642	12.187	12.028	12.135	<b>12.322</b>
9	0.9	9.534	12.026	12.120	11.894	<b>12.145</b>
10	1	9.464	11.864	11.995	11.649	<b>12.008</b>
11	2	9.310	11.64	11.601	11.522	<b>11.657</b>
12	3	9.295	11.506	11.520	11.062	<b>11.597</b>

**Figure 8.** Convergence curves of the algorithms.

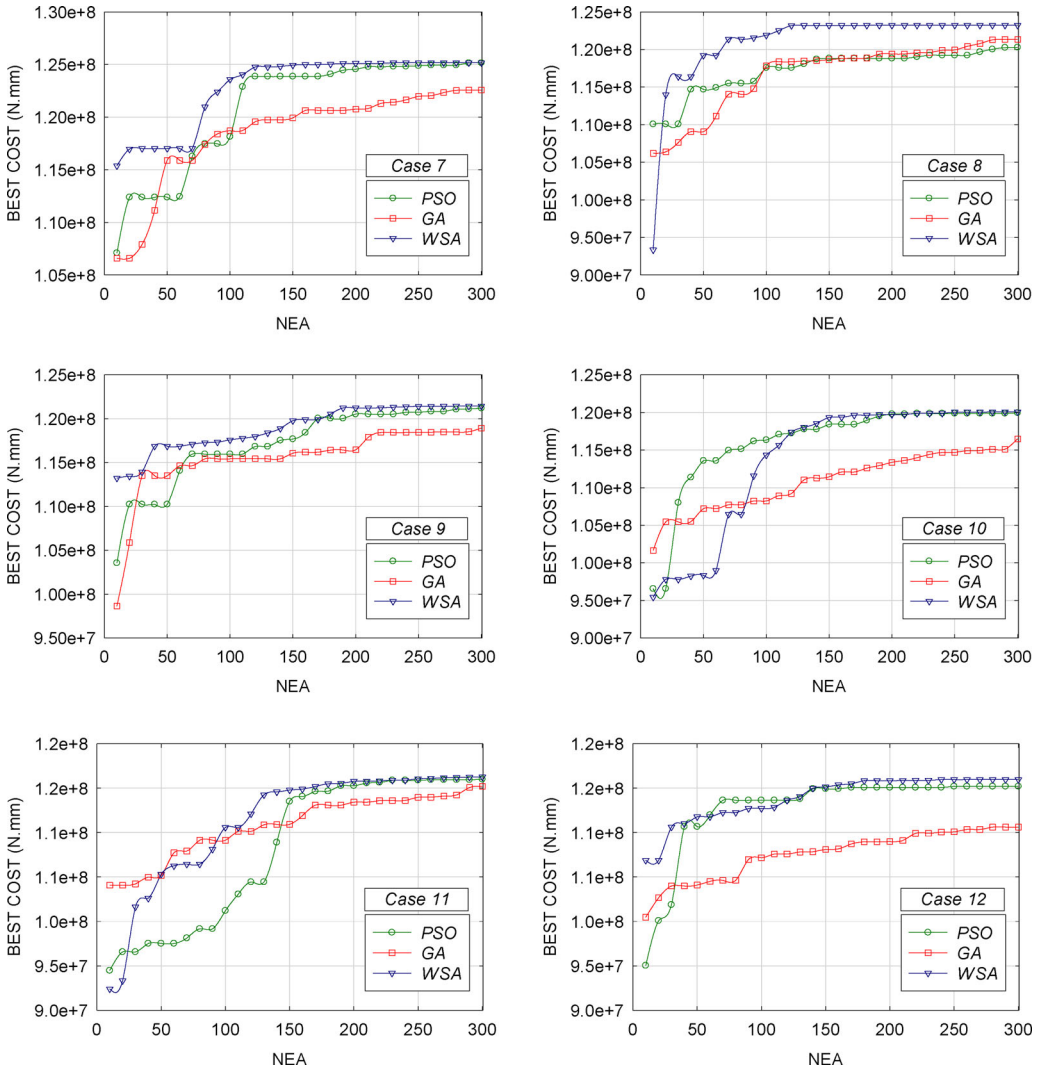


**Figure 8.** Convergence curves of the algorithms.

length of the cylinder  $L$  varies between 1.8 in and 54 in. Here, 12 cases associated with these aspect ratios ( $L/R$ ) are considered. These cases are listed in Table 4, where the best result for each case is written in boldface.

$[0^\circ, \theta^\circ, 90^\circ, -\theta^\circ, -\theta^\circ, 90^\circ, \theta^\circ, 0^\circ]_s$  are the laminate layups of the composite cylinders, where  $\theta$  plies are the plies whose direction needs to be optimized. Seven design variables are considered for the optimization of the fiber path. Moreover, the thickness of each ply is 0.127 mm, and the total thickness of the laminate is 2.032mm. The laminae are assumed to be bonded together perfectly. Also, material constitutive properties of the carbon/epoxy lamina are given in Table 2.

The framework could be equipped with various optimization strategies. In this article, for demonstrating this notable feature, three different optimization algorithms are implemented and introduced to the main code. One novel optimization algorithm, WSA, and GA and PSO, as the most common optimization algorithms, are selected. The settings of GA, PSO, and WSA are the same as those set in Refs. (Simon 2008; Kaveh and Dardas Eslamlou 2020a, 2020b). Accordingly, for the GA, a mutation probability of 0.01, a crossover probability of 1, and roulette wheel

**Table 5.** Optimized orientation angle distribution obtained by each algorithm.

Case	Algorithm	$T_1$ (°)	$T_2$ (°)	$T_3$ (°)	$T_4$ (°)	$T_5$ (°)	$T_6$ (°)	$T_7$ (°)
1	PSO	11.113	0.590	24.555	3.938	0.000	36.178	47.958
	GA	0.577	13.427	47.683	7.002	0.000	21.148	36.259
	WSA	0.107	0.000	71.641	27.332	0.503	38.742	50.494
2	PSO	0.000	1.637	50.523	3.276	0.000	38.935	49.295
	GA	0.142	0.600	79.873	5.467	0.000	40.450	52.137
	WSA	0.000	0.000	70.137	0.000	0.000	41.559	50.265
3	PSO	2.006	0.000	84.209	5.773	18.543	48.337	53.319
	GA	20.207	1.119	53.798	28.427	6.755	41.597	41.271
	WSA	0.221	4.470	0.000	0.000	20.644	47.993	53.633
4	PSO	3.050	6.831	24.294	3.286	25.879	49.827	55.890
	GA	2.989	0.000	76.347	15.564	14.285	46.535	41.948
	WSA	0.000	0.024	37.659	0.000	28.133	49.115	56.707
5	PSO	6.460	0.000	41.471	38.887	22.262	49.183	50.951
	GA	25.125	0.845	55.877	13.773	23.407	49.543	53.588
	WSA	0.000	4.642	49.525	29.922	23.255	48.898	52.796
6	PSO	6.328	4.940	47.242	50.955	22.053	49.017	52.630
	GA	11.639	17.210	37.274	53.313	23.346	45.960	53.888
	WSA	6.001	0.029	41.422	9.920	25.553	53.658	53.384
7	PSO	0.808	0.000	28.542	4.889	29.423	49.877	52.955
	GA	2.077	3.635	80.700	28.218	29.314	43.983	57.424
	WSA	0.000	0.000	2.432	1.092	29.693	48.830	54.263
8	PSO	3.707	1.408	70.353	37.954	27.728	48.565	53.275
	GA	2.645	5.825	54.882	24.478	28.116	46.326	56.338
	WSA	0.000	0.800	58.881	0.520	29.632	47.804	55.169
9	PSO	0.451	0.000	73.788	12.458	26.910	49.027	52.775
	GA	0.163	24.755	68.924	11.850	27.263	49.964	50.844
	WSA	0.870	0.696	90.000	3.426	28.247	49.182	52.683
10	PSO	8.712	0.000	88.026	4.259	27.838	48.148	53.890
	GA	13.279	2.142	39.176	29.492	24.585	48.219	57.147
	WSA	0.000	1.025	65.134	0.174	30.702	48.451	56.842
11	PSO	8.417	1.187	41.436	2.221	32.088	48.282	51.825
	GA	3.498	1.831	50.425	23.064	25.589	52.141	50.289
	WSA	0.764	0.000	78.905	8.362	29.772	49.515	53.180
12	PSO	0.000	9.457	21.278	6.196	32.233	48.224	53.104
	GA	8.902	2.671	55.086	67.097	20.995	51.578	47.925
	WSA	0.127	0.000	60.915	3.979	31.992	46.930	54.008

selection are used. For PSO, a social constant for swarm interaction equal to 1, a cognitive constant of 1, and an inertial constant equal to 0.3 are set.

Furthermore, in WSA, the number of territories is considered 2, according to the original article (Kaveh and Dadras Eslamlou 2020a, 2020b). In all algorithms, the number of populations and the maximum NEA is set to 10 and 300. Buckling performance design using PSO, GA, and WSA optimization algorithms are carried out by the FEM optimization framework on variable-stiffness cylindrical composites having different aspect ratios, separately.

Table 4 provides the optimized buckling load with respect to the aspect ratio  $L/R$  for each algorithm. From Table 4, it can be seen that the optimal buckling load increases significantly as the aspect ratio decreases from 3 to 0.1. That means it is harder to force the shorter cylinders to buckle in comparison with the longer ones. For  $\frac{L}{R} > 1$ , the buckling load reduces to an asymptotic value. The convergence curves of the algorithms for each case are presented in Fig. 8, where the best so far obtained buckling moments (in N mm) are plotted against NEA.

Optimization of the buckling load resulted in an improved FE model with better orientation angle distribution  $T = [T_1, T_2, T_3, T_4, T_5, T_6, T_7]$  for the steered plies. Table 5 gives these orientation angle distributions for the optimized models of each algorithm for all the cases, separately. It could be found that for the part of the cylinder close to the narrow section with  $\theta = T_1$  degree, where is under tension, lower fiber angles (with a median of  $1^\circ$ ) are required to bear the tensile load. On the other hand, the opposite side of the cylinder, where it is close to the narrow section having  $\theta = T_7$ , which is under compression, demands higher values of the orientation

angle (with a median of  $53^\circ$ ). As a result, the distribution of the compressive load in the  $T_7$  side is taking place more appropriately and is transferred more effectively from the  $T_7$  to  $T_1$  section. That leads to higher load-carrying capacity in VS cylinders in comparison to QI cylinders. Also, it can be concluded that the buckling moment has a lower sensitivity to the fiber angles assigned to the middle sections than those assigned to the upper and lower sections.

To compare the maximum buckling loads of VS cylinders with QI cylinders, a column for the QI cases is also provided in Table 4. With a simple comparison between the maximum optimized values obtained by the optimization algorithms and the refereed article, which appears in bold font, and the constant-stiffness ones, which have  $\theta = 45^\circ$  in all their narrow sections, it reveals that the buckling performance of the cylinders has been improved considerably. The improvement percentage in critical load for each case is equal to: 27.64%, 27.11%, 23.58%, 22.04%, 21.37%, 21.71%, 21.66%, 21.75%, 21.50%, 21.19%, 20.13%, 19.85%, respectively.

The values optimized by this framework, in approximately all cases, reported better results than Rouhi et al. (2014). In the present study, optimization was conducted by performing approximately 300 number of function evaluations, while in the referred article, there are several sampling stages, each of which requires 550 structural analyses. After the sampling phase, optimization on the surrogate model was also performed with a population size of 1000 and 10 number of generations. It is also noteworthy that in the metamodeling approach, the results are always accompanied by some errors.

## 6. Conclusion

In summary, we developed and utilized an ABAQUS/MATLAB interface for the analysis and optimal design of VS cylindrical composites subjected to bending-induced buckling moments. Different cases for the length to radius aspect ratios are considered for the VS composite cylinder in order to show the applicability of the framework. The radius of the cylinder at the top and bottom ends are equal to 457.2 mm. However, the length of the cylinder  $L$  varies between 45.72 and 1371.6 mm. Also,  $[0^\circ, \theta^\circ, 90^\circ, -\theta^\circ, -\theta^\circ, 90^\circ, \theta^\circ, 0^\circ]_s$  are the laminate layups of the composite cylinders, where  $\theta$  plies are the plies whose direction needs to be optimized. For this purpose, seven design variables for the path function were considered. It is shown that nearly all of the parameters involved in the finite element modeling phase of the script could be easily customized to meet the researchers' needs. In this study, a recently developed algorithm – the so-called Water Strider Algorithm (WSA) – is applied as one of the novel optimization metaheuristics to show the versatility of the framework in the optimization stage. Buckling loads are maximized for all of the aspect ratios, separately. Commercial finite element analysis (FEA) software ABAQUS was used for the buckling analysis of the cylindrical composites for the mechanical properties given in Table 2.

The following blocks of the python-script could be readily customized to meet the researchers' needs:

- Dimensions of the cylinder (length  $L$  and diameter  $D$ )
- The number of design variables  $m$ . The values of narrow sections  $NS$  and  $n$  might need to be changed accordingly.  $m$  represents the number of design variables, and  $n$  is the number of narrow sections between each of the two subsequent  $T_i$  s. Also,  $NS$  is the total number of narrow sections.
- Material properties
- Number of desired critical buckling loads (`numEigen`)
- Loading
- Boundary condition

In comparison to the results provided in the literature, it is observed that this framework not only does reach better results but also reduces the computational cost significantly. The sensitivity of the load-bearing capacity of optimally designed cylinders to middle section angles is examined. The results show that the buckling load is highly sensitive to the top and bottom angles rather than side angles. This mechanical interpretation of the results, in addition to its applicability in industry sectors, can be put into practice in the development of new optimization methods for VS cylinders. For example, an intelligent new method can adaptively distribute the computational cost to update the fiber angles considering their sensitivity.

This framework can perform optimization task satisfactorily, more specifically, for lower aspect ratios ( $\frac{L}{R} < 2$ ). The applicability of the approach can be extended to data generation for high-fidelity surrogate models such as deep neural networks (DNN).

## Disclosure statement

The author(s) declared no potential conflicts of interest with respect to the research, authorship, and/or publication of this article.

## Funding

The author(s) received no financial support for the research, authorship, and/or publication of this article.

## ORCID

M. Azimi  <http://orcid.org/0000-0001-7406-6721>

## References

- Alidoost, H., and J. Rezaeepazhand. 2017. Instability of a delaminated composite beam subjected to a concentrated follower force. *Thin-Walled Structures* 120:191–202. doi:10.1016/j.tws.2017.08.032.
- Barbero, E. J. 2013. *Finite element analysis of composite materials using Abaqus™*. Boca Raton, FL: CRC Press.
- Blom, A. W., B. F. Tatting, J. M. A. M. Hol, and Z. Gürdal. 2009. Fiber path definitions for elastically tailored conical shells. *Composites Part B: Engineering* 40 (1):77–84. doi:10.1016/j.compositesb.2008.03.011.
- Ehsani, A., and J. Rezaeepazhand. 2016. Stacking sequence optimization of laminated composite grid plates for maximum buckling load using genetic algorithm. *International Journal of Mechanical Sciences* 119:97–106. doi:10.1016/j.ijmecsci.2016.09.028.
- Geng, X., L. Zhao, and W. Zhou. 2020. Finite-element buckling analysis of functionally graded GPL-reinforced composite plates with a circular hole. *Mechanics Based Design of Structures and Machines* 1–17. doi:10.1080/15397734.2019.1707688.
- Ghayoor, H., M. Rouhi, S. V. Hoa, and M. Hojjati. 2017. Use of curvilinear fibers for improved bending-induced buckling capacity of elliptical composite cylinders. *International Journal of Solids and Structures* 109:112–22. doi:10.1016/j.ijsolstr.2017.01.012.
- Ghiasi, H., K. Fayazbakhsh, D. Pasini, and L. Lessard. 2010. Optimum stacking sequence design of composite materials. Part II: Variable stiffness design. *Composite Structures* 93 (1):1–13. doi:10.1016/j.compstruct.2010.06.001.
- Ghiasi, H., D. Pasini, and L. Lessard. 2009. Optimum stacking sequence design of composite materials. Part I: Constant stiffness design. *Composite Structures* 90 (1):1–11. doi:10.1016/j.compstruct.2009.01.006.
- Gürdal, Z., and R. Olmedo. 1993. In-plane response of laminates with spatially varying fiber orientations-variable stiffness concept. *AIAA Journal* 31 (4):751–8. doi:10.2514/3.11613.
- Gürdal, Z., B. F. Tatting, and C. K. Wu. 2008. Variable stiffness composite panels: Effects of stiffness variation on the in-plane and buckling response. *Composites Part A: Applied Science and Manufacturing* 39 (5):911–22. doi:10.1016/j.compositesa.2007.11.015.
- Holland, J. H. 1992. *Adaptation in natural and artificial systems: An introductory analysis with applications to biology, control, and artificial intelligence*. Cambridge, MA: MIT Press.

- Hosseini, K., M. Safarabadi, M. Ganjiani, E. Mohammadi, and A. Hosseini. 2020. Experimental and numerical fatigue life study of cracked AL plates reinforced by glass/epoxy composite patches in different stress ratios. *Mechanics Based Design of Structures and Machines* 1–17. doi:10.1080/15397734.2020.1714448.
- Hu, H.-T., and H.-C. Chen. 2018. Buckling optimization of laminated truncated conical shells subjected to external hydrostatic compression. *Composites Part B: Engineering* 135:95–109. doi:10.1016/j.compositesb.2017.09.065.
- Hyer, M. W., and H. H. Lee. 1991. The use of curvilinear fiber format to improve buckling resistance of composite plates with central circular holes. *Composite Structures* 18 (3):239–61. doi:10.1016/0263-8223(91)90035-W.
- Kaveh, A., A. Dadras, and N. Geran Malek. 2019a. Optimum stacking sequence design of composite laminates for maximum buckling load capacity using parameter-less optimization algorithms. *Engineering with Computers* 35 (3):813–32. doi:10.1007/s00366-018-0634-2.
- Kaveh, A., A. Dadras, and N. Geran Malek. 2019b. Robust design optimization of laminated plates under uncertain bounded buckling loads. *Structural and Multidisciplinary Optimization* 59 (3):877–91. doi:10.1007/s00158-018-2106-0.
- Kaveh, A., and A. Dadras Eslamlou. 2020a. Water strider algorithm: A new metaheuristic and applications. *Structures* 25:520–41. doi:10.1016/j.istruc.2020.03.033.
- Kaveh, A., and A. Dadras Eslamlou. 2020b. *Metaheuristic optimization algorithms in civil engineering: New applications*. Switzerland: Springer.
- Kaveh, A., A. Dadras Eslamlou, N. Geran Malek, and R. Ansari. 2020. An open-source computational framework for optimization of laminated composite plates. *Acta Mechanica* 231 (6):2629–50. doi:10.1007/s00707-020-02648-0.
- Kennedy, J., and R. Eberhart. 1995. Particle swarm optimization. Paper presented at Proceedings of ICNN'95 – International Conference on Neural Networks, Perth, WA, Australia, Australia, November 27 to December 1.
- Khalkhali, A., S. Ebrahimi-Nejad, and N. G. Malek. 2018. Comprehensive optimization of friction stir weld parameters of lap joint AA1100 plates using artificial neural networks and modified NSGA-II. *Materials Research Express* 5 (6):066508. doi:10.1088/2053-1591/aac6f6.
- Li, E. 2017. Fast cylinder variable-stiffness design by using Kriging-based hybrid aggressive space mapping method. *Advances in Engineering Software* 114:215–26. doi:10.1016/j.advengsoft.2017.07.004.
- Moussavian, H., and M. Jafari. 2017. Optimum design of laminated composite plates containing a quasi-square cut-out. *Structural and Multidisciplinary Optimization* 55 (1):141–54. doi:10.1007/s00158-016-1481-7.
- Muc, A., and A. Ulatowska. 2010. Design of plates with curved fibre format. *Composite Structures* 92 (7):1728–33. doi:10.1016/j.compstruct.2009.12.015.
- Oromiehie, E., B. G. Prusty, P. Compston, and G. Rajan. 2019. Automated fibre placement based composite structures: Review on the defects, impacts and inspections techniques. *Composite Structures* 224:110987. doi:10.1016/j.compstruct.2019.110987.
- Paris, A. J. 2009. Bending of two-ply cord composite cylindrical shells. *Mechanics Based Design of Structures and Machines* 37 (3):283–98. doi:10.1080/15397730902845057.
- Parnas, L., S. Oral, and Ü. Ceyhan. 2003. Optimum design of composite structures with curved fiber courses. *Composites Science and Technology* 63 (7):1071–82. doi:10.1016/S0266-3538(02)00312-3.
- Qablan, H. A., S. Rabab'ah, B. A. Alfoul, and O. A. Hattamleh. 2020. Semi-empirical buckling analysis of perforated composite panel. *Mechanics Based Design of Structures and Machines* 1–18. doi:10.1080/15397734.2020.1784198.
- Qin, H., Z. Liu, Y. Liu, and H. Zhong. 2017. An object-oriented MATLAB toolbox for automotive body conceptual design using distributed parallel optimization. *Advances in Engineering Software* 106:19–32. doi:10.1016/j.advengsoft.2017.01.003.
- Ribeiro, P., H. Akhavan, A. Teter, and J. Warmiński. 2014. A review on the mechanical behaviour of curvilinear fibre composite laminated panels. *Journal of Composite Materials* 48 (22):2761–77. doi:10.1177/0021998313502066.
- Rouhi, M., H. Ghayoor, S. V. Hoa, and M. Hojjati. 2014. Effect of structural parameters on design of variable-stiffness composite cylinders made by fiber steering. *Composite Structures* 118:472–81. doi:10.1016/j.compstruct.2014.08.021.
- Rouhi, M., H. Ghayoor, S. V. Hoa, and M. Hojjati. 2015. Multi-objective design optimization of variable stiffness composite cylinders. *Composites Part B: Engineering* 69:249–55. doi:10.1016/j.compositesb.2014.10.011.
- Rouhi, M., H. Ghayoor, S. V. Hoa, and M. Hojjati. 2017. Computational efficiency and accuracy of multi-step design optimization method for variable stiffness composite structures. *Thin-Walled Structures* 113:136–43. doi:10.1016/j.tws.2017.01.019.
- Rouhi, M., H. Ghayoor, S. V. Hoa, M. Hojjati, and P. M. Weaver. 2016. Stiffness tailoring of elliptical composite cylinders for axial buckling performance. *Composite Structures* 150:115–23. doi:10.1016/j.compstruct.2016.05.007.
- Setoodeh, S., M. M. Abdalla, and Z. Gürdal. 2006. Design of variable-stiffness laminates using lamination parameters. *Composites Part B: Engineering* 37 (4-5):301–9. doi:10.1016/j.compositesb.2005.12.001.



- Shahgholian-Ghahfarokhi, D., G. Rahimi, M. Zarei, and H. Salehipour. 2020. Free vibration analyses of composite sandwich cylindrical shells with grid cores: Experimental study and numerical simulation. *Mechanics Based Design of Structures and Machines* 1–20. doi:10.1080/15397734.2020.1725565.
- Simon, D. 2008. Biogeography-based optimization. *IEEE Transactions on Evolutionary Computation* 12 (6):702–13. doi:10.1109/TEVC.2008.919004.
- Sivanandam, S., and S. Deepa. 2008. *Genetic algorithms. Introduction to genetic algorithms*, 15–37. Berlin-Heidelberg: Springer.
- Systèmes, D. 2010. *Abaqus 6.10: Analysis user's manual*. Providence, RI: Dassault Systèmes Simulia Corp.
- Tauzowski, P., B. Blachowski, and J. Lógó. 2019. Functor-oriented topology optimization of elasto-plastic structures. *Advances in Engineering Software* 135:102690. doi:10.1016/j.advengsoft.2019.102690.
- White, S. C., P. M. Weaver, and K. C. Wu. 2015. Post-buckling analyses of variable-stiffness composite cylinders in axial compression. *Composite Structures* 123:190–203. doi:10.1016/j.compstruct.2014.12.013.
- Wu, Z., P. M. Weaver, G. Raju, and B. Chul Kim. 2012. Buckling analysis and optimisation of variable angle tow composite plates. *Thin-Walled Structures* 60:163–72. doi:10.1016/j.tws.2012.07.008.
- Zuo, W. 2013. An object-oriented graphics interface design and optimization software for cross-sectional shape of automobile body. *Advances in Engineering Software* 64:1–10. doi:10.1016/j.advengsoft.2013.04.003.